

# A QSO survey via optical variability and zero proper motion in the M 92 field

## IV. More QSOs due to improved photometry

J. Brunzendorf\* and H. Meusinger \*

Thüringer Landessternwarte Tautenburg, D-07778 Tautenburg  
e-mail: brunz@tls-tautenburg.de, meus@tls-tautenburg.de

**Abstract.** We continue the QSO search in the 10 square degrees Schmidt field around M 92 based on variability and proper motion (VPM) constraints. We have re-reduced 162 digitised  $B$  plates with a time-baseline of more than three decades and have considerably improved both the photometric accuracy and the star-galaxy separation at  $B > 19$ . QSO candidates are selected and marked with one out of three degrees of priority based on the statistical significance of their measured variability and zero proper motion. Spectroscopic follow-up observations of 84 new candidates with  $B > 19$  revealed an additional 37 QSOs and 7 Seyfert 1s. In particular, all 92 high-priority candidates are spectroscopically classified now; among them are 70 QSOs and 9 Seyfert 1s (success rate 86%). We expect that 87% (55%) of all QSOs with  $B < 19.0$  (19.8) are contained in this high-priority subsample. For the combined sample of high-priority and medium-priority objects, a completeness of 89% is estimated up to  $B_{\text{lim}} = 19.5$ . The sample of all AGNs detected in the framework of the VPM search in the M 92 field contains now 95 QSOs and 14 Seyfert 1s with  $B \leq 19.9$ . Although the VPM QSOs were selected by completely different criteria, their properties do not significantly differ from those of QSOs found by more traditional optical survey techniques. In particular, the spectra and the optical broad band colours do not provide any hints on a substantial population of red QSOs up to the present survey limit.

**Key words.** Galaxies: active – Galaxies: Seyfert – Galaxies: statistics – quasars: general –

### 1. Introduction

The number of known QSOs is growing very rapidly. Over the last decade, among others, the Durham/AAT survey (Boyle et al. 1990), the Large Bright Quasar Survey (Hewett et al. 1995), the Edinburgh Quasar Survey (Goldschmidt & Miller 1998), and the Hamburg/ESO survey (Wisotzki et al. 2000) have been completed. Presently, the 2dF Quasar Survey (Croom et al. 2001) and the Sloan Digital Sky Survey (Schneider et al. 2001) are extremely efficient at identifying very large numbers of quasars. The INT Wide Angle Survey (Sharp et al. 2001) is expected to detect a statistically significant sample of high-redshift quasars. Very deep quasar samples were obtained in the Lockman hole via the X-ray satellite ROSAT (Hasinger et al. 1998) and in the optical domain with the Hubble Space Telescope (e.g., Conti et al. 1998), respectively. Further, the VLA FIRST Bright Quasar Survey (e.g., White et al.

2000) will define a radio-selected QSO sample that is competitive in size with current optically selected samples. All these surveys select the QSO candidates on the basis of their particular colours with respect to stars and galaxies or their brightness at X-ray or radio wavelengths. In other words, they rely on the different broad-band spectral energy distribution (SED) as the prime selection criterion.

Despite the large number of QSOs now catalogued, the selection effects of the conventional surveys are not yet fully understood (see, e.g., Webster et al. 1996; White et al. 2000; Gregg et al. 2002). It is therefore important to perform alternative QSO surveys using selection criteria that do not directly rely on the shape of the SED. Variability and zero proper motion are such criteria. We started a variability and proper motion (VPM) survey based on several hundred digitised Schmidt plates (Meusinger et al. 2002). Due to the special demands on the number and the time-baseline of the available observations such an attempt must be limited to comparatively small and confined areas.

We perform the VPM search in two fields of a size of ten square degrees each, centered on the globular clusters

\* Visiting Astronomer, German-Spanish Astronomical Centre, Calar Alto, operated by the Max-Planck-Institute for Astronomy, Heidelberg, jointly with the Spanish National Commission for Astronomy

M 3 and M 92, respectively. The work in the M 92 field is the subject of the present series of papers. In Paper 1 (Brunzendorf & Meusinger 2001), we described the observational material, the photometric and astrometric data reduction, and the selection procedure of the QSO candidates. The QSO sample resulting from the spectroscopic follow-up observations of these candidates was presented in Paper 2 (Meusinger & Brunzendorf 2001). In Paper 3 (Meusinger & Brunzendorf 2002), the properties of the narrow-emission line galaxies among the VPM QSO candidates are discussed.

Both the completeness and the efficiency of the VPM search primarily depend on the photometric accuracy (see Paper 1). From the comparison with other optical QSO samples we find that the previous VPM QSO sample is virtually complete for brighter magnitudes, but its completeness drops rapidly at the faint end ( $B > 19$ ). In the context of the work on Paper 3, we have refined substantial parts of the reduction of all digitised plates with the result of a significantly improved sample of QSO candidates at fainter magnitudes. In the present paper, we present the results of the follow-up spectroscopy and discuss the properties of the enlarged VPM QSO sample.

In Sect. 2, we briefly describe the major revisions of the data reduction procedure. The new candidate selection and the selection effects are the subjects of Sect. 3. The new spectroscopic follow-up observations are described in Sect. 4. Section 5 deals with the newly detected QSOs and the properties of the enlarged QSO sample. Finally, conclusions are given in Sect. 6. As in the previous papers, we adopt  $H_0 = 50 \text{ km s}^{-1} \text{ Mpc}^{-1}$  and  $q_0 = 0$ .

## 2. Revised data reduction

In the present paper, the same observational material is used as in Papers 1 and 2, namely a selection of 208 photographic plates taken with the Tautenburg Schmidt telescope in the years 1963 – 1997 and digitised by means of the Tautenburg Plate Scanner. The plates, the digitisation, and the reduction procedures have been presented at length in Paper 1. Here we describe the revised photometric reduction of the 162 plates taken in the Johnson  $B$  system. There are two major revisions made: we apply a more powerful software package both for the object search and for the determination of the object parameters, and we average over the measurements from plates of nearly the same epoch. The astrometric data, on the other hand, are taken from the previous study.

Motivated by the results of extensive tests we decided to replace our previously used reduction software package by the SExtractor package (Bertin & Arnouts 1996). These tests have clearly shown that the SExtractor detects faint objects, on our plates, with a much higher reliability. In other words, it reaches a higher completeness at faint magnitudes with less false detections caused by the grain noise of the photographic emulsion. In addition, its photometric (but not its astrometric) accuracy proved to be better at faint magnitudes.

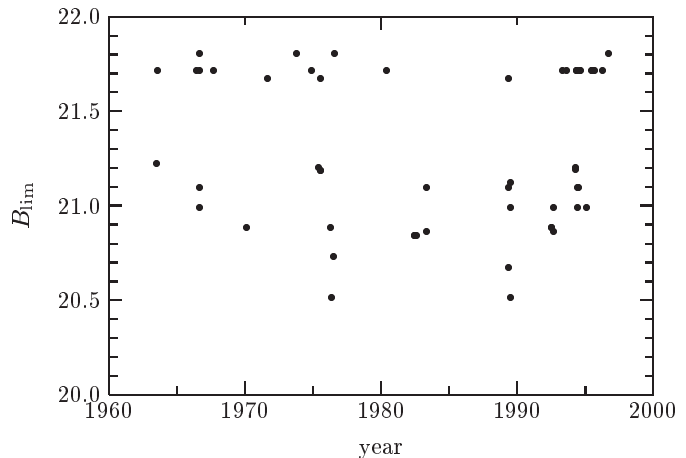


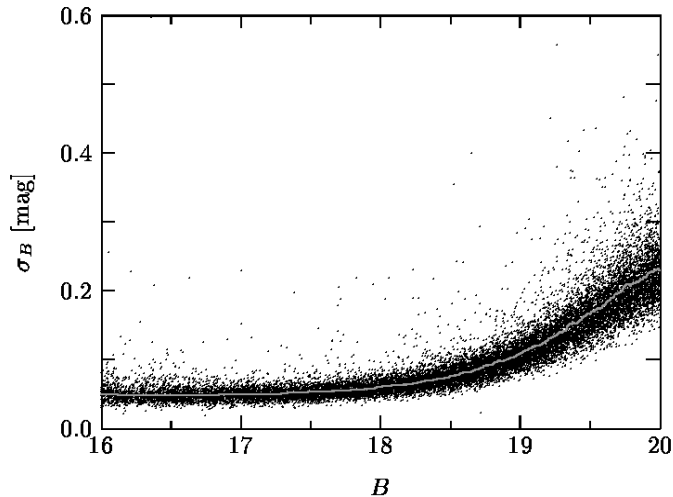
**Fig. 1.** Limiting magnitudes  $B_{\text{lim}}$  of the re-reduced photometric data of all 54 epochs.

The digitisation yields the photographic transparencies  $t$  of the respective plate which have to be transformed into photometric densities  $d = -\log_{10} t$  to provide suitable input data for the object search realized by the SExtractor. For each plate, in a first run the full width at half maximum ( $FWHM$ ) of the star-like sources is derived. The object detection is then done on the image convolved with a Gaussian of the same  $FWHM$  to maximize the detection sensitivity (see the documentation of the SExtractor package for details). The final determination of the object parameters (position, magnitude aso.), however, is done on the original, i.e. unfiltered, image. SExtractor typically detects about 30% more real sources than our previously used software. The resulting basic object sample, defined in exactly the same way as described in Paper 1, therefore contains now more than 42 200 objects. The additional objects have faint magnitudes down to  $B = 21$ . For the present, however, we are primarily interested in a high completeness of the total VPM QSO sample. The main aim of the present study is to complete the QSO sample in the M 92 field to the limiting magnitude  $B_{\text{lim}} \approx 19.7$  from Papers 1 and 2. For this magnitude range, the new sample of objects is essentially identical with the original sample from Paper 1. The discussion of the selection effects from Paper 1 remains largely valid; modifications due to the improved photometric accuracy are discussed in Sect. 3.2. The investigation of the additional objects has to be deferred to a prospective study.

The photometric calibration of the revised internal magnitudes was done in exactly the same way as outlined in Paper 1. The revised photometry yields limiting magnitudes of the plates in the range of  $B_{\text{lim}} = 19 - 22$ , where  $B_{\text{lim}}$  is identified with the  $B$  magnitude of the faintest standard star detected. In order to obtain a maximum sensibility with respect to faint variable objects, it is advisable to minimize the impact of the different photometric accuracies and limiting magnitudes of the individual plates caused by the scatter in their qualities. For this reason, we only consider plates that match *all* of the following

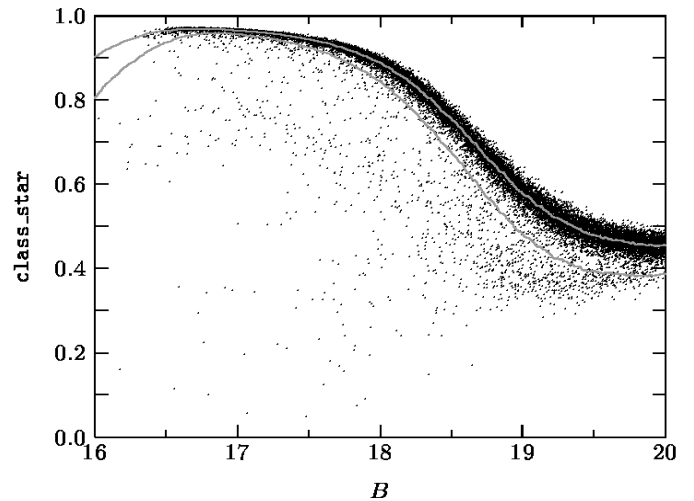
**Table 1.** Selection criteria and number of QSO candidates for the medium- and high-priority, respectively, subsamples.

criterion	high-priority QSO candidates	medium-priority QSO candidates
proper motion	$I_\mu \leq 3$	$I_\mu \leq 4.3$
overall variability	$I_\sigma \geq 2$	$I_\sigma \geq 1.645$
long-term variability	$I_\Delta \geq 2$	$I_\Delta \geq 1.645$
mean $B$ magnitude	$18 \leq B \leq 19.8$	$18 \leq B \leq 19.8$
remark		without high-priority objects
number of candidates	92	53
classified in Paper 2	52 (49 QSOs+Seyfert 1, 3 stars)	5 (3 QSOs+Seyfert 1, 1 NELG, 1 star)
remaining	40	48

**Fig. 2.** Photometric standard deviation  $\sigma_B$  of the magnitudes  $B_i$  measured for each star-like object on the plates  $i$  as a function of the mean magnitude  $B$ . The curve represents the median value.

criteria: (1.) limiting magnitude  $B_{\text{lim}} \geq 19.8$ , (2.) number of detected objects  $N \geq 30000$ , and (3.) plates taken at zenith distances  $z \leq 45^\circ$ . These criteria are satisfied by 116  $B$  plates. We aim at a photometric accuracy of better than  $\sim 0.1$  mag at  $B = 19$  and better than  $\sim 0.2$  mag at  $B = 20$ . In order to reach this aim, we averaged 18 pairs of plates of close-by epochs as well as 10 triples of plates of adjacent epochs. In addition, we excluded further 26 plates from our data sample, since in these cases plates of the same or close-by epochs yet significantly better quality are available. The final photometric data set comprises 54 epochs spanning 33.2 years, where each single plate matches the quality constraints defined above. An overview over the final epochs and limiting magnitudes  $B_{\text{lim}}$  is given in Fig. 1. The mean accuracy of the photometric measurements of each object is shown in Fig. 2. The comparison with Fig. 5 in Paper 1 indicates a substantial reduction of the photometric errors, especially for  $B > 19$ . The calculation of the new indices for overall variability  $I_\sigma^{\text{new}}$  and long-term variability  $I_\Delta^{\text{new}}$  strictly follows the descriptions given in Paper 1. In the following, we refer to these new variability indices as  $I_\sigma$  and  $I_\Delta$  without the

index <sup>new</sup>. Note however, that the values of these indices are not identical with the data given in Papers 1 and 2.

**Fig. 3.** Classification parameter `class_star` for all measured objects in the magnitude range  $B = 16 - 20$ . The curves represent the median value (upper) and the  $5\sigma$  deviation from the median (lower).

An effective star-galaxy separation is a further important requirement for an efficient candidate selection, mainly because deviations from the star-like appearance may produce additional photometric errors that can mock variability (Paper 3). In our first attempt (Paper 1), image profile indices were derived on the basis of the relation between radii and magnitudes measured on a deep  $R$  plate. The SExtractor package allows a more sophisticated morphological classification based on a trained neural network. Moreover, in Paper 3, we have stressed that the classification should be done on exactly the same plates which are used for photometry and/or astrometry. In the present study, we use the index `class_star` computed by SExtractor from the measurements on the  $B$  plates. An object is considered stellar if `class_star`  $< 0.4$ , which roughly corresponds to a  $5\sigma$  deviation from the median value in the relevant magnitude range  $19 \leq B \leq 19.8$  (Fig. 3). In this way, the star-galaxy separation is substantially improved.

### 3. QSO candidate selection and selection effects

#### 3.1. QSO candidate selection

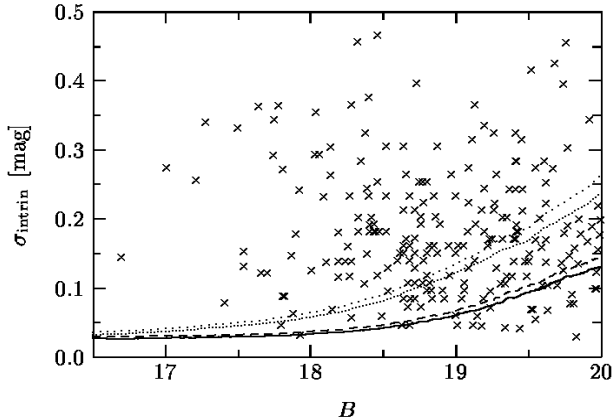


**Fig. 4.** Standard deviation of the intrinsic magnitude fluctuation,  $\sigma_{\text{intrin}}$ , versus apparent mean  $B$  magnitude for the QSOs ( $\times$ ) from Hook et al. (1994). The curves indicate the detection limits  $\sigma_{\text{intrin}}^{\text{min}}$  of the present paper for  $I_{\sigma} \geq 2$  (dashed) and  $I_{\sigma} \geq 1.645$  (solid), respectively. For comparison, detection limits from Paper 1 are given (dotted lines).

As in Paper 1, an object is considered a QSO candidate if it shows a star-like image structure (see above) and a proper motion index  $I_{\mu} \leq 4.3$ . Objects in the dense cluster region (distance to the centre of M 92  $r \leq 6'$ ) or near the border of the field (distance to the border  $r \leq 10$  mm) as well as the brightest ( $B < 13$ ) and faintest ( $B > 19.8$ ) objects were excluded. The remaining 7 090 of all 34 500 objects form the QSO candidate sample. It is expected that *all* QSOs with  $13 < B < 19.8$  in the field are recorded in this sample. Note that till now no variability constraint is applied.

Among all QSO candidates, a high-priority subsample as well as a medium-priority subsample are selected according to the constraints given in Table 1. The remaining QSO candidates are of only low priority, since they have no significant variability. Yet they are of special interest in conjunction with other QSO selection criteria, e. g., based on colour, when one focuses on the completion of the sample of known QSOs in the field. The magnitude limit  $18 \leq B \leq 19.8$  for the high- and medium-priority candidates is motivated by the fact that, in this paper, we aim at an increase of the completeness at faint magnitudes. In Papers 1 and 2, we have selected and classified high- and medium-priority candidates with  $B \geq 16.5$ . In the context of the evaluation of the selection effects in Paper 1 as well as by a direct comparison with the mean QSO surface density from other surveys (Paper 2), we have shown that our QSO sample is virtually complete, at least for  $B \leq 18$ . In the present paper, we consider therefore only candidates with  $B \geq 18$ . The slight increase in the magnitude limit  $B_{\text{lim}}$  from 19.7 (Paper 1) to 19.8 is

justified by the better photometric accuracy at faint magnitudes. Among the remaining low-priority candidates, a number of objects might be of special interest as well. These objects do either meet the classical colour selection criteria, e. g. show a UV excess, and/or failed only one of the variability criteria.

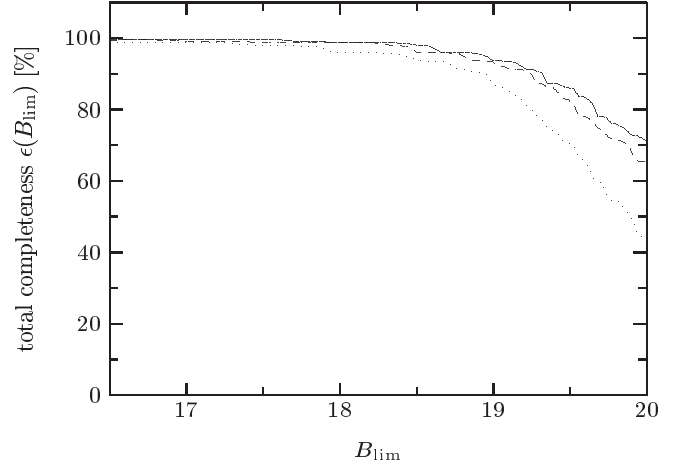


**Fig. 5.** Expected total completeness  $\epsilon(B_{\text{lim}})$  of the present survey up to a given limiting magnitude  $B_{\text{lim}}$ . It is assumed that the QSO candidate selection is based on the  $I_{\sigma}$  criterion only with  $I_{\sigma} \geq 2$  (dashed curve) and  $I_{\sigma} \geq 1.645$  (solid curve), respectively. The dotted indicates the estimated completeness for the selection criterion  $I_{\Delta} \geq 2$  derived from a simple model assuming sinusoidal brightness fluctuations with periodicities  $T \approx 3$  yr. In that case, all objects with periodicities  $T \lesssim 30$  yr also meet the criterion  $I_{\sigma} \geq 2$ .

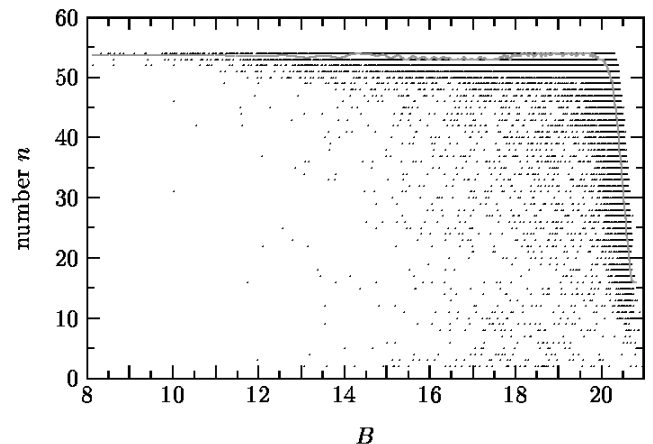


**Fig. 6.** Number of observations  $n$  for each object as a function of its mean apparent magnitude  $B$ . The tight correlation is illustrated by the median curve (solid).

**Table 2.** Additional QSOs and Seyfert 1 galaxies from the present study. In the columns on the right hand side, the index defined in paper 1 for proper motion ( $I_\mu$ ) as well as the newly calculated overall variability index  $I_\sigma$  and long-term variability index  $I_\Delta$  are given.

no	$\alpha$ (J2000)	$\delta$ (J2000)	$z$	$M_B$	$B$	$\overline{U - B}$	$\overline{B - V}$	$I_\mu$	$I_\sigma$	$I_\Delta$
QSO										
66	17 08 46.18	44 08 39.7	1.544	-25.8	19.6	-0.66	0.52	1.19	9.05	3.14
67	17 09 42.45	42 53 14.4	0.705	-23.8	19.7	-0.49	0.10	1.23	4.53	1.45
68	17 10 01.16	43 25 48.2	2.155	-26.7	19.9	-0.82	0.04	2.06	6.25	3.80
69	17 10 52.64	43 15 05.9	0.749	-24.0	19.7	-1.19	0.39	3.09	2.08	2.34
70	17 10 55.63	42 53 09.5	1.088	-24.9	19.8	-0.87	0.04	2.46	4.04	3.57
71	17 11 23.89	43 48 37.7	1.838	-26.7	19.1	-0.50	0.06	2.77	0.78	2.08
72	17 12 00.57	43 29 44.2	1.457	-25.9	19.3	-1.13	0.17	1.91	5.15	2.20
73	17 12 26.39	41 42 12.0	1.148	-25.1	19.8	-0.76	-0.32	0.43	4.95	2.88
74	17 13 08.81	42 08 11.4	2.300	-27.0	19.6	-0.58	0.51	1.91	4.07	4.95
75	17 13 10.63	43 48 55.6	2.484	-27.1	19.7	-0.53	0.47	2.15	2.38	3.54
76	17 13 11.19	42 51 54.2	0.959	-24.7	19.7	-0.75	0.12	0.89	3.89	3.82
77	17 13 20.88	44 15 31.1	0.887	-24.7	19.3	-1.06	0.35	2.86	5.83	1.90
78	17 14 02.85	42 44 22.8	1.494	-25.8	19.5	-0.82	0.05	1.90	6.11	2.79
79	17 14 04.14	43 22 36.4	1.565	-25.8	19.8	-0.76	0.16	1.27	7.93	4.88
80	17 15 00.59	42 54 39.4	1.508	-26.0	19.5	-0.52	-0.15	1.35	4.41	4.24
81	17 15 32.18	43 47 59.4	0.923	-24.6	19.5	-0.83	0.27	1.64	3.28	3.63
82	17 15 40.06	42 42 26.8	1.835	-26.3	19.7	-0.97	-0.02	0.30	-1.51	1.82
83	17 16 05.82	43 30 26.8	2.898	-27.9	19.8	-0.40	0.39	0.24	1.73	3.14
84	17 17 13.20	44 21 04.7	0.607	-23.2	19.8	-1.15	0.43	0.75	4.78	3.08
85	17 17 32.55	43 56 55.6	0.677	-24.0	19.3	-0.98	0.34	0.84	4.73	2.97
86	17 17 36.75	44 23 26.9	1.606	-25.9	19.7	-1.09	0.47	0.88	6.23	4.21
87	17 17 36.95	42 16 53.8	1.847	-26.4	19.6	-1.22	0.57	1.30	2.49	3.42
88	17 18 24.00	42 25 47.7	1.688	-26.2	19.5	-0.82	0.38	2.28	1.12	2.75
89	17 19 12.04	44 11 22.1	1.782	-26.5	19.4	-0.75	-0.33	0.87	2.12	2.42
90	17 19 12.23	43 20 44.7	2.603	-28.1	18.9	-0.18	-0.14	1.12	6.63	3.43
91	17 19 15.42	44 22 46.9	0.420	-23.4	18.6	-0.69	0.30	1.94	12.08	2.02
92	17 19 42.87	43 09 27.1	3.199	-28.7	19.5	1.51	1.11	0.77	7.87	4.28
93	17 19 52.94	41 43 39.5	1.484	-25.7	19.8	-0.67	0.63	0.49	6.03	2.88
94	17 20 04.81	41 47 44.1	1.218	-25.1	19.8	-0.90	0.36	3.16	6.66	3.24
95	17 20 11.02	43 46 34.9	1.459	-25.5	19.9	-1.59	0.56	1.96	4.45	4.09
96	17 21 17.57	43 01 27.0	0.526	-23.2	19.5	-0.75	0.26	0.95	0.05	1.81
97	17 21 42.18	42 44 32.5	2.306	-26.9	19.4	-0.53	0.11	2.08	4.12	2.11
98	17 22 03.06	43 41 06.3	1.069	-25.1	19.4	-1.00	0.14	2.57	6.83	1.19
99	17 23 21.49	43 29 03.3	2.030	-26.5	19.9	-0.69	-0.31	2.87	6.61	3.41
100	17 23 45.96	44 03 27.2	1.749	-26.0	19.7	-0.87	-	1.38	5.40	3.93
101	17 24 01.51	43 20 30.5	1.463	-25.7	19.7	-0.83	0.50	1.01	3.14	4.28
102	17 24 14.22	42 10 47.2	0.748	-24.0	19.5	-1.07	0.42	0.38	6.20	3.03
Sy 1										
103	17 11 39.81	42 14 51.5	0.175	-20.9	19.5	-0.26	1.43	1.78	8.45	3.74
104	17 14 45.16	42 20 27.4	0.337	-22.2	19.5	-1.09	0.27	1.40	7.48	2.59
105	17 16 06.82	44 08 35.9	0.439	-22.8	19.4	-0.93	-0.27	1.62	6.54	3.70
106	17 18 20.94	42 49 13.6	0.166	-21.3	18.7	-0.60	0.41	3.44	24.71	4.67
107	17 19 11.96	42 10 48.0	0.169	-20.6	19.7	-0.34	1.26	2.48	9.14	3.11
108	17 19 36.63	42 45 29.1	0.284	-21.9	19.5	-0.89	0.83	0.85	3.33	3.81
109	17 21 53.87	42 33 36.3	0.209	-21.7	18.9	-0.75	0.72	2.15	8.96	2.59

### 3.2. Selection effects

With respect to the better photometric accuracy and the reduced number of epochs we repeat here the estimation of the completeness rates outlined in Paper 1. In Fig. 4, we compare the intrinsic magnitude fluctuations measured by Hook et al. (1994) for a large samples of conventionally selected QSOs with the detection limits of the present study. For now we only consider the incompleteness caused by

the application of the overall variability criterion  $I_\sigma > 2$ , or  $I_\sigma > 1.645$ , respectively. Considering the Figs. 20 and 21 in Paper 1, which refer to the variability properties of the Hook-QSOs, Eq. (23) in Paper 1, and the photometric accuracy of our revised data (Fig. 2), we derived the revised completeness rates for the selection based on  $I_\sigma$ . The results are shown in Fig. 5. A direct comparison with Fig. 19 in Paper 1 clearly reveals an improved completeness at faint magnitudes. Now, more than 74% of all QSOs

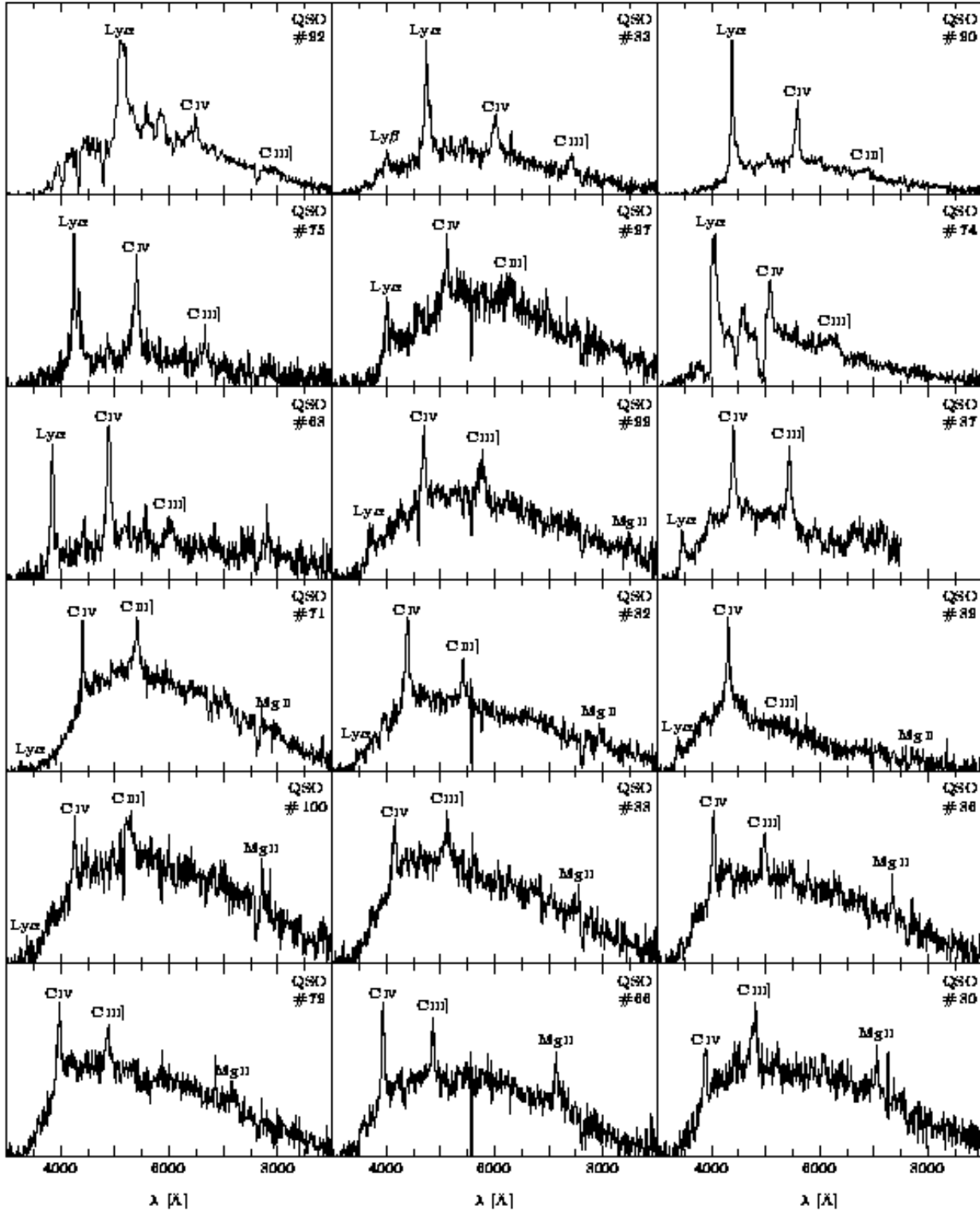


Fig. 7. Low-resolution spectra (uncalibrated flux  $f_\lambda$  versus wavelength  $\lambda$ ) of all QSOs and Seyfert 1s from the present study. In the upper right corner of each panel, the object type and the running number from Tab. 2 are given.

brighter than  $B_{\text{lim}} = 19.7$  are expected to be included in the high-priority candidate subsample ( $I_\sigma > 2$ ), compared to only 64% in Paper 1. Due to the better photometric accuracy, the expected completeness at  $B_{\text{lim}} = 20$  amounts to 65%, compared with previously 52% (Paper 1).

The number of epochs is, of course, significantly smaller than in Paper 1 (54 *versus* 152). Nevertheless, this reduction is not expected to provide a substantial selection effect: for objects brighter than  $B = 20$ , the number of photometric data points is sufficiently constant (Fig. 6). Thus, the impact of the varying number of epochs on the

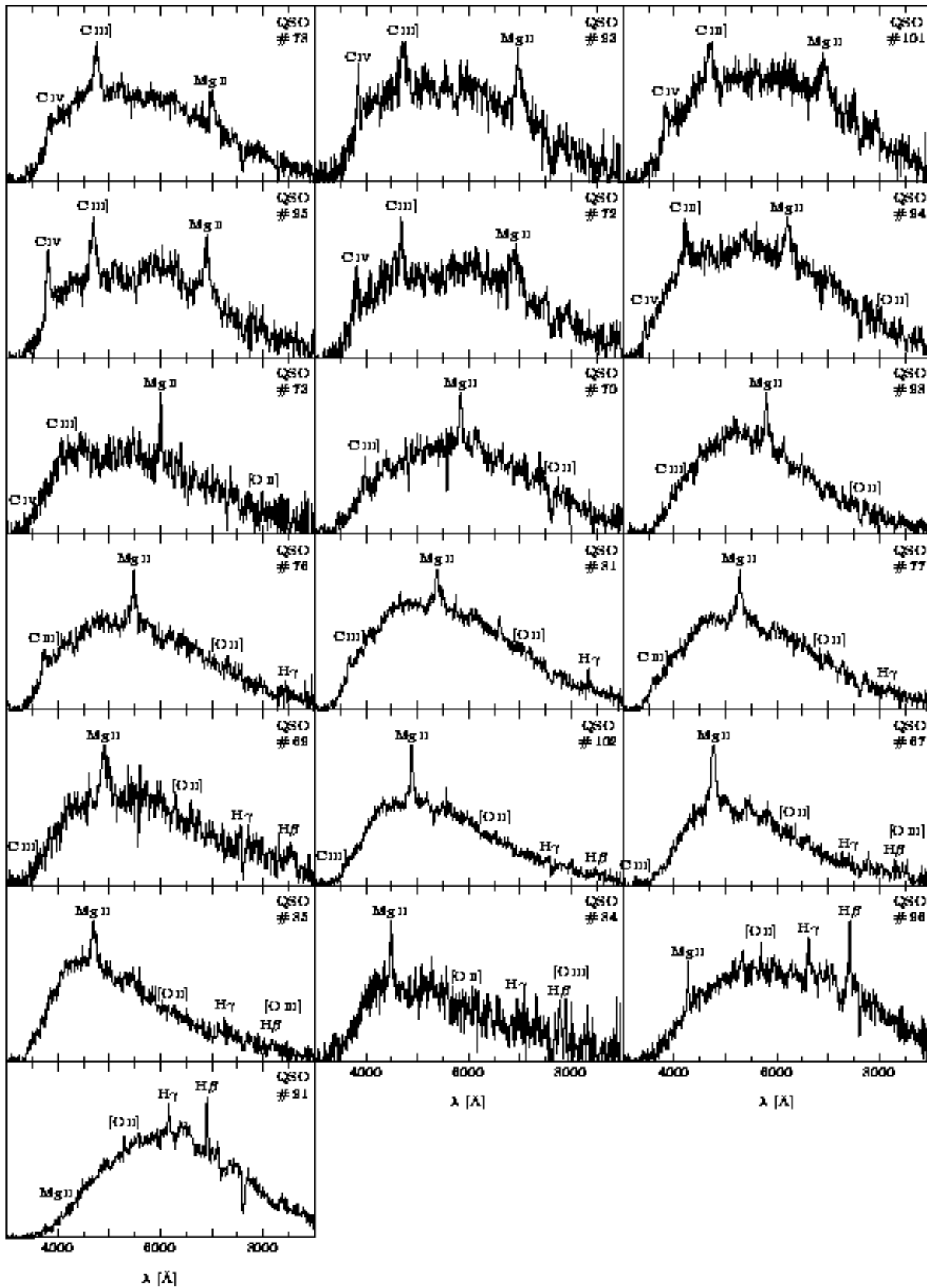


Fig. 7. (continued)

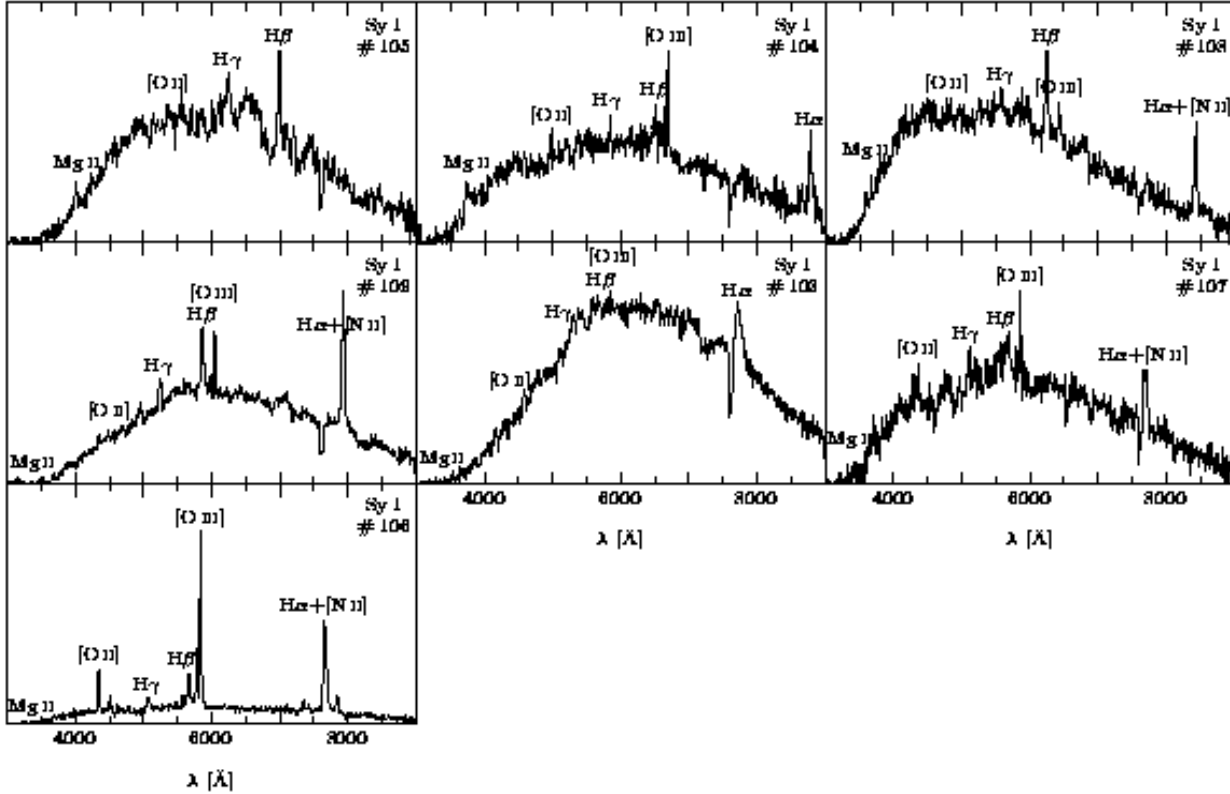


Fig. 7. (continued)

total selection effects is negligible for  $B \leq 20$ . Note that at  $B \approx 20$  the mean number of data points is about 50 in this paper as well as in Paper 1, yet the photometric accuracy is significantly higher in this paper.

The investigation of the selection effects caused by the application of the long-term variability index  $I_{\Delta}$  is not as simple as for the overall variability index  $I_{\sigma}$ , since it depends not only on the amplitude of the intrinsic variability of the object in units of the photometric accuracy at this magnitude, but also on the shape of the lightcurve, in particular on the dominating time-scale of the variability. We applied similar simple model simulations as described in Paper 1 to illustrate the influence of  $I_{\Delta}$ . Lightcurves are calculated for the 54 epochs of the present study assuming a sinusoidal process with periodicity  $T$  superimposed on white noise. The variability indices  $I_{\sigma}$  and  $I_{\Delta}$  directly result from the chosen values of  $T$  and the amplitude of the sinusoidal in units of the noise. If  $T \lesssim 30$  yr, the selection of the QSO candidates is defined by the constraint  $I_{\Delta} \geq 2$ , since in this case the overall variability is always  $I_{\sigma} > 2$ . In order to provide at least an estimate for the incompleteness caused by the selection criterion  $I_{\Delta} \geq 2$  we assumed a typical time-scale of  $T \approx 3$  yr (observer frame). The resulting completeness rates are shown in Fig. 5.

#### 4. Spectroscopic follow-up observations

Spectroscopic follow-up observations of the new QSO candidates were performed again with CAFOS at the 2.2 m telescope on Calar Alto, Spain. During six nights in July,

2001, low-resolution spectra were taken with the B-400 grism and a SITE1d CCD. The weather conditions were good, partly photometric, with the exception of a cloudy last night. The strategy of the observations closely followed the procedures of the 1998 and 1999 campaigns (Paper 2). Depending on the seeing of  $1'' \dots 2''$ , a slit width of  $1''.2 \dots 1''.7$  was chosen, equivalent to an effective linear resolution of  $22 \dots 31 \text{ \AA}$ . At the beginning of each night, calibration lamp spectra were taken to provide information for the data reduction, in particular for the wavelength calibration.

In total, 84 new QSO candidates of the M 92 field were successfully observed, namely:

- (a) all 40 remaining high-priority candidates,
- (b) 9 further candidates that match all requirements for the high-priority subsample except that they are slightly fainter than  $B = 19.8$ ,
- (c) 23 of the 48 medium-priority candidates, among them all objects fainter than  $B = 19$  as well as all objects with  $U - B \leq -0.4$ ,
- (d) all 10 low-priority candidates fainter than  $B = 19.0$  that have at least one variability index,  $I_{\sigma}$  or  $I_{\Delta}$ , greater than 1.645 and meet the colour selection criterion given by Scholz et al. (1997),
- (e) 2 low-priority candidates that meet the colour selection criterion by Scholz et al. (1997).

The reduction of the spectra was done under ESO-MIDAS using the long-slit spectroscopy package LONG. As in Paper 2, we abstained from a flux calibration. The clas-



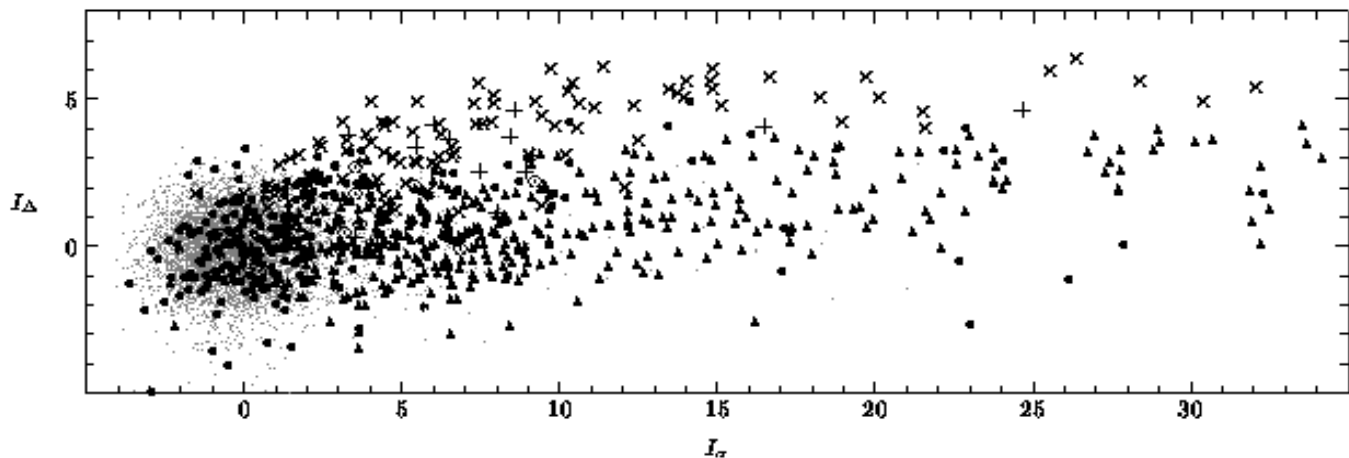


**Fig. 8.** Long-term variability index  $I_{\Delta}$  versus overall variability index  $I_{\sigma}$  for all QSO candidates with  $B \geq 16.5$  (gray dots), established QSOs ( $\times$ ), Seyferts ( $+$ ), NELGs ( $*$ ), spectroscopically identified stars ( $\bullet$ ), visually identified galaxies ( $\blacktriangle$ ), and visual double stars ( $\odot$ ).

sification of all candidates with spectroscopic follow-up observations was done as described in Paper 2. In one case (J171926.5+432123, not contained in Table 2) we could not unambiguously classify the spectrum due to the poor signal-to-noise ratio. With only one emission line, without clear evidence for a broad line component, it could have been a QSO at  $z = 1.6$  or a galaxy at  $z = 0.12$ . Since the object appeared fuzzy and slightly elongated on the acquisition image, we classified it as galaxy. In all other cases the classification is based on at least two emission and/or absorption lines in the respective spectrum. We also cross-checked if the classification is in general agreement with the visual morphological classification on the acquisition frames.

## 5. Properties of the extended QSO sample

The follow-up spectroscopy revealed an additional 37 QSOs and 7 Seyfert 1s among the 84 observed candidates. The redshifts, magnitudes, colours, and indices are listed in Table 2 in a similar style as in Paper 2. A search in the NED has shown that the Seyfert 1 no. 106 was previously known as FBQS J171820.9+424914 with  $z = 0.167$  (White et al. 2000). No other identifications with objects of known redshift were found. The QSO no. 71 is within less than  $10''$  from the radio sources B3 1709+438 and FIRST J171123.2+434844, and the Seyfert 1 no. 108 is within the error ellipse of the ROSAT source 1RXS 1735.9+424518. At least three further objects (no. 72, 75, 81) can be identified with ROSAT sources from the list of Dahlem & Thiering (2000).

Remarkably, all objects from Table 2 are fainter than  $B = 19$ , in agreement with the fact that the major improvement of the photometry is at the fainter magnitudes (Sect. 3.2). With regard to the spectroscopic observations of the different selection groups listed in the previous Section, the number of newly found QSOs among the candidates observed is itemised as follows: (a) 30

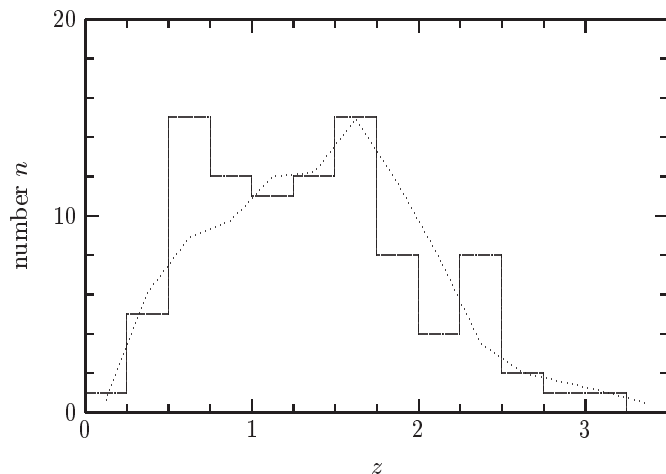


**Fig. 9.** Distribution of the redshifts (number of QSOs per 0.25 redshift bin) for the extended VPM QSO sample (solid). For comparison, the dotted polygon gives the  $z$  distribution for the 3 814 QSOs from the early data release of the SDSS Quasar Catalogue (Schneider et al. 2001), normalised to the number of the VPM QSOs.

QSOs/Seyfert 1s out of 40 objects, (b) 3 out of 9, (c) 5 out of 23, where all five have at least one variability index larger than 2, (d) 6 out of 10, where 4 have one variability index larger than 2, and (e) 0 out of 2.

With the exception of the high-priority subsample, which was completely observed, the sample of the further objects observed may appear somewhat patchy and inconsequent, in particular because the VPM search is partly combined with a colour criterion. The reason for the latter was that it is one of the main intentions of our quasar search to provide a QSO sample useful for the statistical investigation of the long-term variability. For this aim, it is necessary to avoid a substantial bias against low-variability QSOs, if they exist. Nevertheless, variability and zero proper motion are the dominating

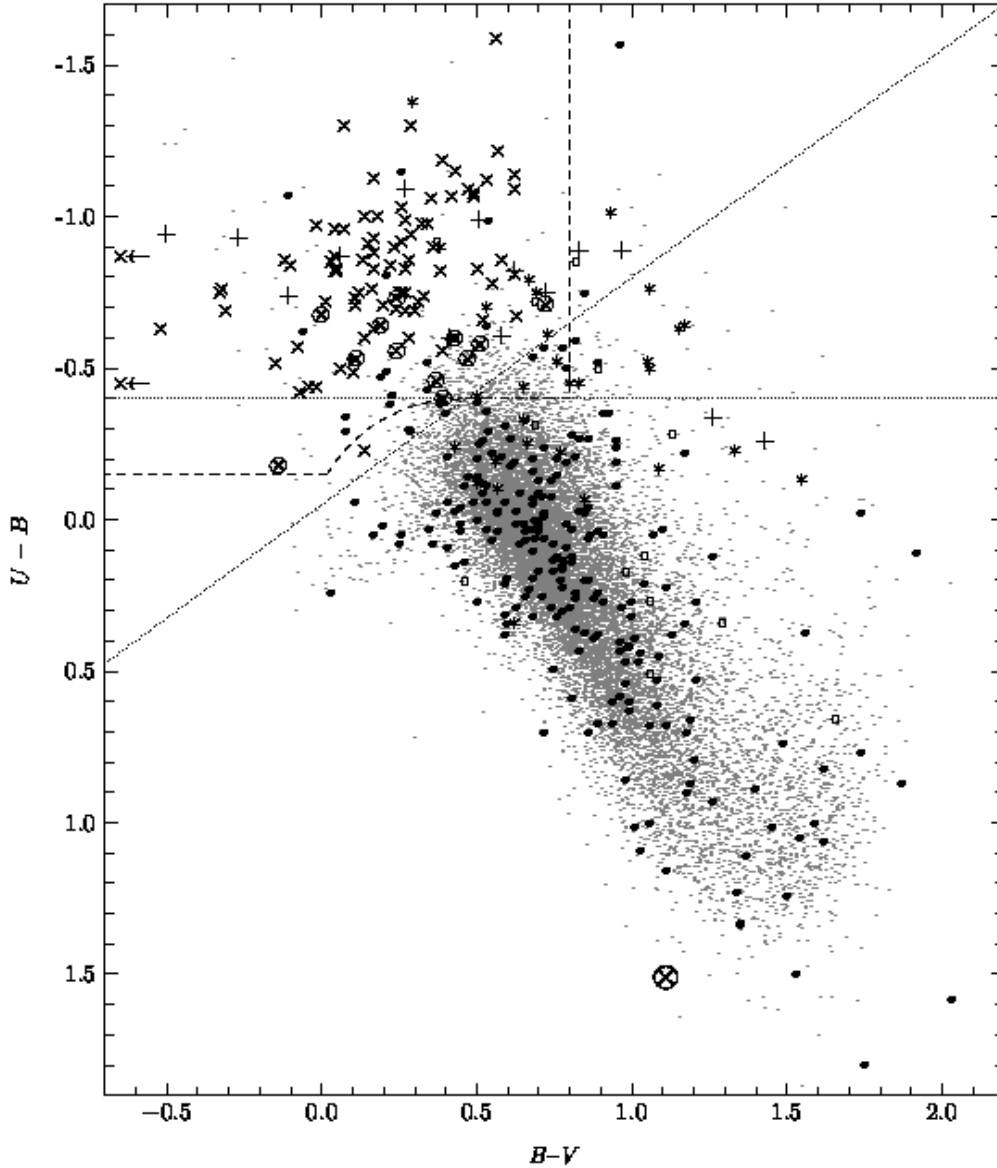


**Fig. 10.** Colour-colour diagram of the QSOs ( $\times$  for  $z < 2.2$ ,  $\otimes$  for  $2.2 \leq z < 3$ ,  $\otimes$  for  $z > 3$ ), the Seyfert 1s (+), and the NELGs (\*). (Two QSOs without measured  $V$  magnitudes are marked by  $\leftarrow$  at the left hand side of the diagram.) In addition, spectroscopically identified stars ( $\bullet$ ) and visual binaries ( $\circ$ ) are shown as well as the non-identified objects with  $B \leq 19$  (small dots). Selection criteria from colour surveys are indicated. *Horizontal dotted line*: UVX search, *diagonal dotted line*: two-colour search as discussed by Scholz et al. (1997), *dashed curve*: two-colour selection according to LaFranca et al. (1992).

constraints for all selection groups but (e), which is however irrelevant. Note also that most (75%) of the newly detected QSOs/Sy1s are found without additional colour constraints and that the statistics mentioned above confirms again the efficiency of the variability selection. An evaluation of the variability indices  $I_\sigma$  and  $I_\Delta$  of all objects classified so far (including those from Paper 2) clearly indicates the distinctive properties of the QSOs/Seyfert 1s (Fig. 8) and confirms again the importance of the long-term variability index for the VPM search.

With these new detections, the extended VPM AGN sample in the M 92 field now contains 95 QSOs and 14 Seyfert 1s. The redshifts of the QSOs span the range from

$z = 0.15$  to  $z = 3.2$ , the majority (83%) have  $z < 2$ . The histogram of the redshifts (Fig. 9) is similar to that for the previous sample (Fig. 6 in Paper 2), except that the fraction of  $z > 2$  QSOs is larger in the new (22%) than in the previous data (14%), as was expected (Paper 2). The general form of the  $z$  distribution is comparable with that from the SDSS Quasar Catalogue I. Early Data Release (Schneider et al. 2001). The  $\chi^2$ -test confirms at a significance level  $\alpha = 0.95$  that the two distributions are not significantly different. In principle, a bias against higher redshifts is expected for the VPM sample due to the empirical anti-correlation between variability and luminosity/redshift (e. g. Hook et al. 1994). Figure 9 suggests that

such a bias is probably not strong in our sample. Both for the VPM sample and the SDSS sample, the distribution has a maximum at  $z \approx 1.6$  and decreases sharply towards higher redshifts. The local maximum at  $z \approx 0.6$  in the VPM sample is probably related to the increase of the survey depth for those  $z$  where the strong Mg II  $\lambda 2798$  line is in the centre of the  $B$  band.

The low-dispersion spectra (in the observer frame) for all objects from Table 2 are shown in Fig. 7. The spectra of several objects show absorption features, most notably the BAL J171308.8+420811 (no.74) and the luminous high-redshift QSO no.92. In other respects, the spectra of the VPM QSOs are not unusual, in agreement with what was found in Paper 2.

In Paper 1, we presented the colour-colour diagram of the QSO candidates which shows a broad scatter of the colour indices and a substantial fraction of red QSO candidates. In Paper 2 (Fig.4), we have shown that all of the high-priority candidates with unusually red colours proved to be foreground stars and, moreover, that all previously established VPM QSOs would have been detected by a classical two-colour search as well. This result remains true for the extended VPM sample, too. There is no object among the QSOs in Table 2 with an unusual position either on the colour-colour diagram (Fig. 10) or on the colour-redshift diagrams (Fig. 11). A fraction of QSOs with redder colours among the VPM-selected objects is expected if (1.) there exists a substantial population of QSOs whose continuum is redder than classical colour-selected AGNs (e. g., Webster et al. 1996; Kim & Elvis 1999; Risaliti et al. 2001; Maiolino et al. 2001), (2.) there is no strict dichotomy of the colour indices, i.e. there also exists a fraction of QSOs that are mildly redder than colour-selected ones and not completely dark in the optical (White et al. 2000; Menou et al. 2001), and (3.) abnormal red QSOs are in general not much less variable than colour-selected QSOs. In this context we note that one explanation of the BAL phenomenon is related to dust-enshrouded QSOs (Voit et al. 1993; Becker et al. 1997; Egami 1999) and that the three VPM QSOs with strongest signs of absorption (no. 3, 74, and 92) all have both strong overall variability and high long-term variability indices. However, the colour indices of these three objects do not significantly deviate from the mean colour- $z$  relation (Fig. 11). In Paper 2, we have estimated that the fraction of red QSOs must be less than 5% for  $B \leq 19.7$ . The re-evaluation on the basis of the extended QSO sample gives an upper limit of 3% for  $B \leq 19.8$ .

The VPM sample covers a brightness range of three magnitudes, from  $B = 16.8$  to 19.9. The cumulative surface density, i.e. the number counts  $N(< B)$  per solid angle for the extended VPM QSO sample is shown in Fig. 12. The  $N(< B)$  roughly follows a power law with an increase of the slope from about 0.6 at brighter magnitudes to about 0.75 for  $B > 18$ , but our sample is probably too small for a discussion of the fine structure of the  $N(< B)$  relation. The main importance of this diagram is to illustrate the completeness of the survey by the com-

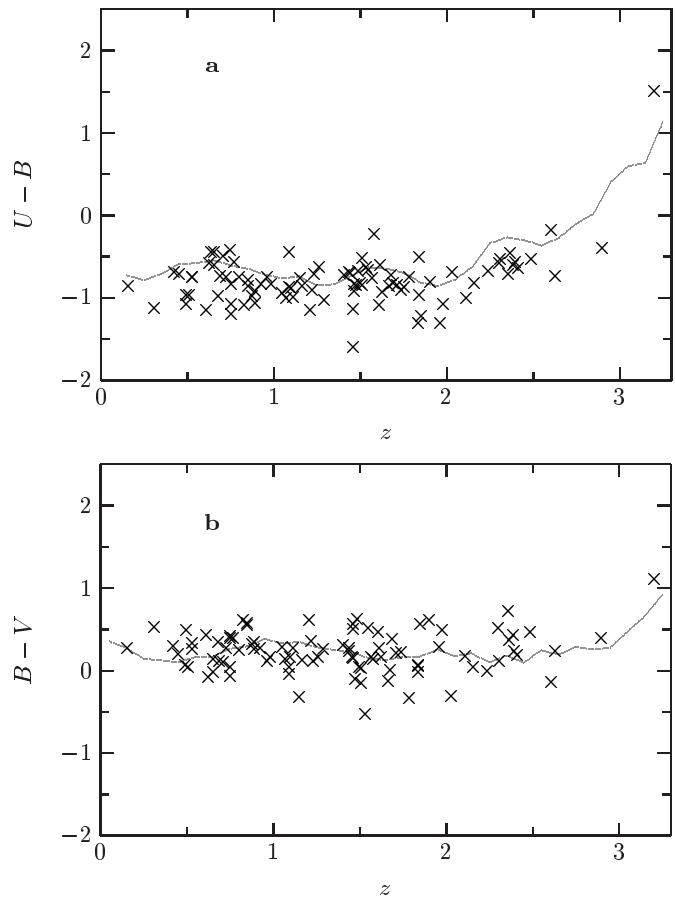


**Fig. 11.** Colour indices  $U-B$  (a) and  $B-V$  (b) of the identified QSOs ( $\times$ ) as a function of the redshift  $z$ . For the sake of comparison, the mean relations for the QSOs from Véron-Cetty & Véron (2001) are plotted.

parison with the number counts from other surveys. For comparison, Fig. 12 shows also the QSO surface density derived by Hartwick & Schade (1990) from a combination of several optical surveys available at that time. A mean relation given by Wisotzki (1998) is also shown. The latter counts have been derived from a combination of more recent QSO surveys, including the LBQS, the AAT, and the Hamburg/ESO survey and are given in the form of a polynomial approximation for  $\log N(B_J)$ . For the transformation into the Johnson  $B$  system we adopted  $B = B_J + 0.1$  for QSOs. There is a good agreement of our number counts with the comparison relations, except for the fact that our surface densities at brighter magnitudes are larger than those given by Hartwick & Schade, as was mentioned already in Paper 2. At  $B \gtrsim 19.5$ , the VPM sample is expected to be substantially incomplete; the incompleteness corrections in Fig. 12 were derived from Fig. 5.

The present VPM search is not suited to detect very close pairs of QSOs since objects have to be separated by at least  $8''$  to be included in our sample as different objects (Paper 1). Despite this restriction, which has of course no significant influence on the efficiency of the search method, we looked for QSO pairs within a search radius of  $2'$ . Two

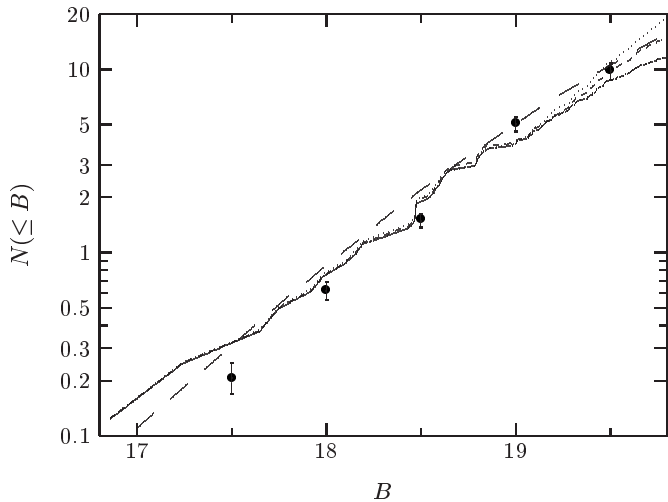


**Fig. 12.** Cumulative QSO surface density  $N(\leq B)$ , i.e. number of QSOs brighter than a given magnitude  $B$  per square degree where  $B$  has been corrected for an interstellar extinction of  $A_B = 0.08$  mag. **Solid curve:** all VPM QSOs, **short-dashed curve:** high-priority VPM QSOs, corrected for incompleteness due to the  $I_\sigma \geq 2$  criterion (Fig. 5), **dotted curve:** high-priority VPM QSOs, corrected for incompleteness due to the combined  $I_\sigma \geq 2$  and  $I_\Delta \geq 2$  criteria assuming periodicities  $T \approx 3$  yr (see text + Fig. 5). Bullets with error bars: integral surface densities from Hartwick & Schade (1990). The long-dashed curve corresponds to an analytical approximation given by Wisotzki (1998) that was derived from a composite optical QSO sample.

pairs were found, however with large separations of  $91''$  (no.5,84) and  $106''$  (no. 49,98), respectively. In both cases, the separations in redshifts are very large.

## 6. Conclusions

In our previous work (Papers 1 and 2), we have described a combined VPM QSO search on 162 digitised Schmidt plates of the M 92 field taken with the Tautenburg Schmidt in the  $B$  band between 1960 and 1997. We have confirmed that this method provides an efficient technique for finding AGNs. The efficiency and the completeness of the VPM survey primarily depends on the photometric accuracy. The previous QSO sample suffered from substantial incompleteness at  $B > 19$ . Therefore, we have revised the reduction of all  $B$  plates on the basis of the SExtractor package (Bertin & Arnouts 1996). Both the photometric accuracy and the star-galaxy separation at  $B > 19$  were substantially improved. The mean photometric accuracy is now  $\sigma \approx 0.1$  mag at  $B = 19$  and  $\sigma \approx 0.2$  mag at  $B = 20$ . With the refined variability indices, a number of new QSO candidates of medium or high priority were selected. Spectroscopic follow-up observations of 84 new candidates revealed an additional 37 QSOs and 7 Seyfert 1s with  $B < 19.9$ . The total VPM sample in the M 92 field now comprises 95 QSOs and 14

Seyfert 1s with  $B \leq 19.9$ . For all these AGNs long-term lightcurves are available with a baseline of more than three decades. Among the 92 high priority QSO candidates with  $18 \leq B \leq 19.8$ , we found 70 QSOs and 9 Seyferts 1s, corresponding to a high success rate of 86%. The completeness of the high-priority subsample is estimated to be about 87% for  $B \leq 19$  and 55% for  $B \leq 19.8$ . A total completeness of 89% is derived for the sample of all QSOs brighter than  $B = 19.5$  from the comparison with the number counts given by Hartwick & Schade (1990). Remarkably, the properties of the VPM QSOs do not significantly differ from those of QSOs found by more traditional optical survey techniques. The deeper VPM sample from the present study confirms the result from Paper 2: the spectra and the optical broad band colour indices do not provide any hints on a substantial population of abnormal red QSOs up to the survey limit.

*Acknowledgements.* This research is based on observations made with the 2.2m telescope of the German-Spanish Astronomical Centre, Calar Alto, Spain. We acknowledge financial support from the *Deutsche Forschungsgemeinschaft* under grants Me1350/8-1 and Me1350/13-1. J.B. acknowledges financial support from the Thüringer Ministerium für Wissenschaft, Forschung und Kunst. We are grateful to L. Wisotzki for sending unpublished material. This research has made use of the NASA/IPAC Extragalactic Database (NED) which is operated by the Jet Propulsion Laboratory, California Institute of Technology, under contract with the National Aeronautics and Space Administration.

## References

- Becker, R.H., Gregg, M.D., Hook, I.M., et al. 1997, ApJ 479, L93  
 Bertin, E., & Arnouts, S. 1996, A&AS 117, 393  
 Boyle, B.J., Fong, R., Shanks, T., et al. 1990, MNRAS 243, 1  
 Brunzendorf, J., & Meusinger, H. 2001, A&A 373, 38 (Paper 1)  
 Conti, A., Kenefick, J.D., Martini, P., et al. 1998, AJ 117, 645  
 Cristiani, S., Trentini, S., LaFranca, F., et al. 1996, A&A 306, 395  
 Croom, S.M., Smith R.J., Boyle, B.J., et al. 2001, MNRAS, 322, L29  
 Dahlem, M., & Thiering, I. 2000, PASP 112, 148  
 Egami, E. 1999, in IAU Symp. 196, Galaxy Interactions at Low and High Redshift, ed. J.E. Barnes & D.B. Sanders (Dordrecht: Kluwer), 475  
 Goldschmidt, P. & Miller, L. 1998, MNRAS 293, 107  
 Gregg, M. D., Lacy, M., White, R., et al. 2002, ApJ 564, 133  
 Hartwick, F.D.A., & Schade, D., 1990, ARA&A 28, 437  
 Hasinger, G., Burg, R., Giacconi, R., et al. 1998, A&A 329, 482  
 Hewett, P.C., Foltz, C.B., & Chaffee, F.H. 1995, AJ 109, 14 98  
 Hook, I.M., McMahon, R.G., Boyle, B.J., et al. 1994, MNRAS 268, 305  
 Kim, D.-W., & Elvis, M. 1999, ApJ 516, 9  
 La Franca, F., Cristiani, S., & Barbieri, C. 1992, AJ 103, 1062  
 Maiolino, R., Salvati, M., Marconi, A., et al. 2001, A&A 375, 25  
 Menou, K., VandenBerk, D. E., Ivezić, Ž., et al. 2001, ApJ 561, 645

- Meusinger, H., & Brunzendorf, J. 2001, A&A 374, 878  
(Paper 2)
- Meusinger, H., & Brunzendorf, J. 2002, A&A, submitted  
(Paper 3)
- Meusinger, H., Brunzendorf, J., Scholz, R.-D., et al. 2002,  
in ASP Conf. Ser., AGN Surveys, Proceedings of IAU  
Colloquium 184, ed. R.F. Green, E.Ye. Khachikian, & D.B.  
Sanders, in press
- Risaliti, G., Marconi, A., Maiolino, R., et al. 2001, A&A 271,  
37
- Schneider, D.P., Richards, G.T., Fan, X., et al. 2001, AJ, in  
press
- Scholz, R.-D., Meusinger, H., & Irwin, M.J. 1997, A&A 325,  
457
- Sharp, R.G., McMahon, R.G., Irwin, M.J., et al. 2001, MNRAS  
326, 45
- Véron-Cetty M.P., & Véron P. 2001, Quasars and Active  
Galactic Nuclei (10th Ed.), A&A 374, 92
- Voit, G.M., Weymann, R.J., & Korista, K.T. 1993, ApJ 95,  
109
- Webster, R.L., Francis, P.J., Peterson, B.A., et al. 1996, Nature  
375, 469
- White, R.L., Becker, R.H., Gregg, M.D., et al. 2000, ApJS 126,  
133
- Wisotzki, L. 1998, Astron. Nachr. 319, 5
- Wisotzki, L., Christlieb, N., Bade, N., et al. 2000, A&A, 358,  
77